Visual system for fast and automated inspection of 3D parts

Flavio Prieto[*,**] — **Tanneguy Redarce**[*]
Richard Lepage[**] — **Pierre Boulanger**[***]

[*]*Laboratoire d'Automatique Industrielle, INSA de Lyon*
20 avenue Albert Einstein, 69621 Villeurbanne, France
Email: {fprieto,redarce}@lai.insa-lyon.fr
[**]*Laboratoire d'Imagerie, de Vision et d'Intelligence Artificielle*
École de Technologie Supérieure, Université du Québec
1100 rue Notre-Dame Ouest, Montréal, Québec, H3C 1K3, Canada
Email: lepage@livia.etsmtl.ca
[***]*Institute for Information Technology, National Research Council of Canada*
Montreal road, building M-50, Ottawa, Ontario, K1A 0R6, Canada
Email: boulanger@iit.nrc.ca

ABSTRACT. *The recent requirement for increased speed in the design and manufacturing of new products led to a rapid evolution of the technics for fast production (rapid prototyping, machining at high speed, etc.). But a significant component did not follow this evolution, that is the dimensional and functional checking process. To automate this significant phase of production, it is necessary to develop some new analysis method. We presented an inspection method designed around three modules: a first one registrates the CAD model of a part and its 3D data obtained with an active optical range sensor, the second module segments the homogeneous cloud of 3D points in areas representing each surface of the object, and the third one is a visual check of the dimensions of the part.*

RÉSUMÉ. *La nécessité récente d'augmenter la vitesse de conception et de réalisation de nouveaux produits a permis de développer de nouvelles techniques de production rapide (prototypage rapide, usinage à très grande vitesse, etc.). Mais un élément non négligeable n'a pas suivi cette évolution, c'est le contrôle dimensionnel et fonctionnel. Afin d'automatiser cette phase importante de la production, il est nécessaire de développer de nouvelles méthodes d'analyse. Dans cet article, nous décrivons la méthode que nous avons développé, elle se compose de trois modules: le premier recale le modèle CAO de la pièce avec les données 3D obtenues par un télémétre laser, le deuxième segmente le nuage de points en surfaces homogénes, et le troisième effectue le contrôle dimensionnel de la pièce.*

KEY WORDS : *Inspection, registration, segmentation, CAD based vision.*

MOTS-CLÉS : *Inspection, recalage, segmentation, systeme de vision CAO.*

1. Introduction

The increasing number of manufactured objects showing complex surfaces, either for functional reason or by design, and technological improvement in manufacturing all create a need for automatic inspection of complex parts. This type of apparatus requires a very accurate geometrical definition of the inspected object, input 3D data with sufficient accuracy, and clearly defined rules for the inspection of these surfaces. Moreover, the development of new manufacturing techniques, such as rapid prototyping or high speed machining, will find their full use only if it is also possible to control the quality as quickly.

The use of three-dimensional coordinate measuring machines and the recent advent of laser sensors combining measurement accuracy and fast acquisition allow obtaining a great number of accurate 3D measurements. These accurate 3D points build up an explicit description of object surfaces. In addition, the corresponding CAD model provides an exact and complete description of the geometry of the object under inspection. We develop a method for automatic inspection of parts including complex surfaces, running from their CAD model (IGES or STL format) and 3D data provided by a telemetric sensor or a coordinate-measuring machine.

At present, it is near to impossible to compare the accuracy obtained with a coordinate measuring machine equipped with a contact sensor (lower than the micrometer) to those delivered by a measuring machine equipped with a laser range finder (about 25 micrometers at best). If one wants to take advantage from the speed of acquisition obtained with a contactless sensor to make systematic dimensional check of complex parts, it is necessary to improve the precision of the depth images obtained with a range finder. In any case, parts manufactured by techniques such as rapid prototyping could be controlled by using the data obtained from a range sensor, because these manufacturing techniques attain accuracy about 0.1 mm at best. The measurements made with a laser telemeters sensor is largely sufficient for the dimensional measurement of objects made by rapid prototyping.

The use of CAD models in inspection is interesting because the model contains an exact specification of the part; they provide well-defined models for inspection. CAD models provide a mathematical description of the shape of an object, including an explicit parameterization of surface shape and an explicit encoding of inter-surface relationships. The database can also be augmented with manufacturing information, including geometric tolerance, quality of surface finish, and manufacturing information. An advantage of using CAD representations for inspection is their high flexibility; it is easier to add a new object to the inspection system before its manufacturing.

CAD model is also useful because it offers the possibility of modeling common defects. It is likely that some of the possible part defects are known *a priori* and therefore can be modeled. The inspection system can attempt to determine the nature of the defect by comparing the observed defect to the model's common defects, and a new defect can be quickly introduced into the database. It should be noted, however, that current CAD packages do not allow including potential defects in the model of a part; they must be modeled separately.

We present in this paper a new method of automatic inspection. This method is made up of three modules: a first one makes the registration between the CAD model of a part and its 3D data obtained with an active optical range sensor, the second module segments the homogeneous cloud of 3D points in area representing each surface of the object, and the third one is concerned with dimensional check and outputs results either in a file or on the screen.

2. Review of Literature

The automatic verification of manufactured object is a very recent concern. The main reason is that to carry out this type of task, it is necessary to have contactless sensors. The digitalization of the image from video camera and later from CCD camera made it possible to obtain information on objects and this at high speed. Quickly one arrives at the limit of these sensors for the analysis of 3D parts, at least in industry, because of their limited precision and the difficulty to recreate the third dimension. The appearance of sensor combining a laser beam and a CCD camera allows the rebuilding of the third dimenssion, without however giving the accuracy obtained with a 3D coordinate measuring machine. The laser telemeter sensor made it possible and attains desired speed and precision. It is at the present time possible to automate the inspection process. At present, few papers servey the use of depth image for inspection. One reason is the lack, up to now, of powerful systems for to the recovery of depth images. Research in industrial automated inspection is limited mostly to 2D systems for the inspection of circuit boards and mask [CHI 82]. Three-dimensional automatic inspection has been limited due to the complexity of the problem.

On the inspection part we can quote the article of Newman and Jain [NEW 95], which is a *survey* of the question, where the problem is tackled from the point of view of luminance images (gray-level or binary), range images or other sensing modalities. They discuss the general benefits and feasibility of automated visual inspection, and presents common approachs to visual inspection and also consider the specification and analysis of dimensional tolerances and their influence on the inspection task.

The system GASP (General Automatic Sensor Planning) designed by Truco *et al* [TRU 97] is used to compute the optimal positions for inspection tasks using known imaging sensor (3D range imaging system for example), and feature-based object models. They used FIR (Feature Inspection Representation) which contains the explicit solution for the sensor positioning problem; optimal viewpoint is defined as a function of feature visibility and measurement reliability. They compute visibility with an approximate model; the reliability of inspection depends on the physical sensors and on the processing software. In this paper they demonstrate a complete inspection session involving 3D-object positioning, optimal sensor position, and feature measurement from the optimal viewpoint [TRU 94].

The system developed by Newman and Jain [NEW 95b] permits the detection of defects in range images of castings. This system uses CAD model data for surface classification and inspection. The authors report several advantages for the use of range

images in inspection, namely that they are insensitive to ambient light, the objects can usually be extracted from their background more easily, measurement of depth is accurate, and most important, they are explicitly related to surface information. The authors show the interest for the use of the CAD database in order to carry out the task of inspection. Moreover they show the weakness of the current CAD systems to make automatic check.

In [TAR 95], Tarbox and Gottschlich report a method based on comparing a volumetric model of reference object to a volumetric model of an actual object iteratively created from sensor data. To provide a framework for the evaluation of volumetric inspection, they have developed a system called IVIS (Integrated Volumetric Inspection System). They obtain a volumetric image of the defect by using custom comparison operators between the reference model and the model of the inspected part.

In [MAR 91], Marshall *et al* report a vision system which outputs dense depth data of a part, and the processing algorithm of an array of these data in order to achieve the goal of automatic inspection of mechanical parts, by developing general model-based inspection strategies that can be applied to a large set of objects.

In the previous works, the dimensional control is driven on the whole part. But in inspection tasks, generally one is interested to control only some surfaces of the part. Therefore, in this work, we segmented the 3D image using its CAD model, and thus were able to achieve the visual control on each surface of the piece, in a independent way.

We have worked for several years on measurement verification by comparing CAD models and range images [MOR 96], [BOU 96]. We shown that the size of the defects which can be detected depends in a very significant way on the resolution of the sensor. Therefore we experiment with good 3D-measurement sensor [BER 95], having capability to detect as small defects as 0.05 mm of depth.

3. The 3D laser camera

The basic geometry of 3D laser camera is based on the synchronization of the projection of a laser beam with its return path. The main advantage of this approach is to simultaneously obtain high resolution and large field of view contrary to standard triangulation geometries where a compromise is made between resolution and field of view [RIO 84], [RIO 87], [RIO 97].

The synchronized scanning geometry is based on a doubled-sided mirror that is used to project and detect a focused or collimated laser beam The source used in NRCC prototypes is a laser, which is typically coupled to an optical fiber. A scanning mirror and a fixed one are used to project the laser beam on the scene. The scattered light is collected through the same scanning mirror used for the projection and focused to a linear CCD (Figure 1). Note that the CCD is tilted (Scheimpflug condition) to compensate for defocusing at the detection.

With careful optical design, the divergence of the laser beam can be made to match the resolving element field of view of the CCD linear array. In such conditions, the

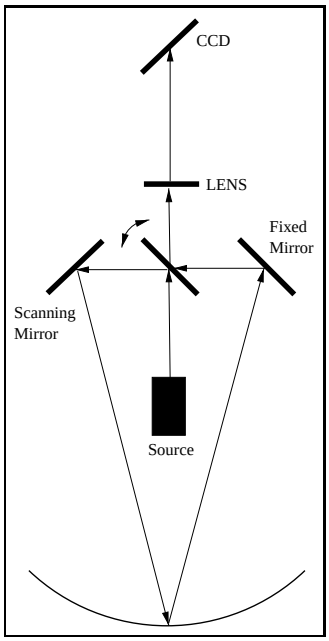

FIG. 1: *Optical principle of the NRCC range sensor*

parameters of the focused laser beam are kept constant over a large depth of view. This property combined with the Scheimpflug condition allow 3D digitizing from very short distance (0.1 meters) to large distance (10 meters) without refocusing or modification algorithm [1].

Essentially the configuration illustrated on the Figure 1 is a profile measurement device. A second scanning mirror (not shown in the illustration) can be used to deflect orthogonally both the projected and the reflected laser beam or the whole camera arrangement can be mechanically translated by commercially available gantry positioning device such as coordinate measuring machines (CMM).

4. The registration method

The registration of two shapes is defined as finding the 3D rigid transformation (rotation + translation) to be applied on one of the shape to bring it into one common cartesian coordinate system with the other one. The registration process in this paper relies on the well-known work of Besl and McKay [BES 92] who in 1992 developed a general-purpose representation method for the accurate and computationally efficient registration of 3D shapes, including free-form curves and surfaces. The method is

1. The explanation of optical principle can be obtained from NRCC web site at http://www.vit.iit.nrc.ca/

based on the Iterative Closest Point (ICP) algorithm, which requires only to find the closest point from a geometric entity to a given point. The rigid transformation is computed using a unit quaternion. But as the transformation estimate is done by a Mean Square (MS) distance computation, this method is not robust to outliners points, generated either by noise or by the presence of other parts in the scene. As a solution to this problem, Masuda and Yokoya [MAS 95] estimate the rigid motion between two range images in a robust way by fusing the ICP algorithm with random sampling and Least Median of Squares (LMS) estimation. They demonstrated that registration between two images can be achieved with a high level of robustness (up to 50 %) to occlusion and noise. Moron [MOR 96b] implemented an algorithm for registration between an unordered cloud of 3D points and a CAD model in STL or IGES format. In the registration process, Moron use the CAD model in STL format rather than in IGES format, so that few precision is lost but computation time is largely improved.

The registration method can be break down into three main steps:

1) The algorithm randomly selects N_S 3D points from the original 3D data set, and then computes a rigid transformation by using an ICP algorithm on the subset. This process is repeated N_T times. To find a solution fot this non-linear problem, we just take a sample of N_S points. The probability of finding a solution increases when N_S decreases or N_T increases. After each ICP execution, the quality of the estimated rigid transformation is evaluated by computing the median square error.

2) The best estimated rigid transformation corresponding to the least median square error is applied over the whole 3D data, and the original 3D data set is segmented into inlier or outlier point sets.

3) A standard mean square ICP algorithm is then applied over the inlier set of points to find the optimal rigid transformation solution.

In order to find a global solution, it may be necessary to apply this method several times, with different initial conditions. From now, we only consider the solution corresponding to best estimate.

4.1. *The LMS algorithm*

The mean square (MS) estimator gives an estimate of the transformation matrix that minimizes the sum of squared distances between the point set and the model. Unfortunately any outlier point in the 3D point set can bias the solution. On the other hand, the least median square estimator finds a solution which minimizes the median of squared distances between the 3D data set and the model. This category of estimator was first introduced by Rousseuw and Leroy [ROU 87] and is theoretically robust up to a proportion of 50% of outliers.

The LMS algorithm is as follows :

1) A subsample P_{RS}^I of N_S 3D points is randomly extracted from the cloud of 3D points R^I:

$$P_{RS}^I \leftarrow RS(R^I, N_S)$$

2) The P_{RS}^{I} subsample is used by the ICP algorithm with the model shape R^{II} to compute the transformation parameters:

$$T_{ICP,n} \leftarrow ICP(P_{RS}^{I}, T_{LMS}, R^{II}).$$

3) The quality of the transformation is then evaluated by a median estimator: $MS(R^{I}, T_{ICP,n}, R^{II})$ with

$$MS(R^{I}, T, R^{II}) = \sqrt{med_{r_i^I \in R^I}(d(T(r_i^I), R^{II})^2)},$$

where d is the point to CAD model distance.

4) If $MS(R^{I}, T_{ICP,n}, R^{II}) < MS(R^{I}, T_{LMS}, R^{II})$ then $T_{LMS} \leftarrow T_{ICP,n}$.

4.2. *The ICP algorithm*

The ICP algorithm can efficiently estimate the rigid transformation between the subsample P_{RS}^{I} and the model shape R^{II}. The algorithm can be divided into two main phases: The first phase consists of finding, for each point from P_{RS}^{I}, its closest point from R^{II}. Phase two computes the rigid transformation between the two associated point sets, using the quaternion representation. Those two operations are repeated until P_{RS}^{I} and R^{II} are sufficiently close. The iterative process stops when $d_{k-1} - d_k < \tau\sigma$ where $d_k = d(P^{I}, P^{II})$ is the sum of squared distances P_i^{I} and P_i^{II}. The threshold value τ represents the convergence tolerance. The scale value σ is used to make the convergence condition dimensionless. It represents the approximate size of P_{RS}^{I} and is defined as the square root of the trace of the covariance matrix of P_{RS}^{I}. For the ICP algorithm, it was demonstrated [BES 92] that the mean squared errors d_k sequence decreases for each iteration monotonically.

The ICP algorithm is the following :

1) $k \leftarrow 1$; $P^{I} \leftarrow T_{LMS}(P_{RS}^{I})$; $d_0 \leftarrow \infty$.

2) Points correspondence is established:

$$P^{II} \leftarrow C(P^{I}, R^{II}).$$

3) Rigid transformation between P^{I} and P^{II} is estimated using quaternion representation:

$$T_{ICP} \leftarrow Q(P_{RS}^{I}, P^{II}).$$

4) Estimated transformation is applied on P_{RS}^{I}:

$$P^{I} \leftarrow T_{ICP}(P_{RS}^{I}).$$

5) $d_k = d(P^{I}, P^{II})$

6) Steps 2 to 5 are repeated untill $d_{k-1} - d_k < \tau\sigma$ with $k \leftarrow k + 1$.

5. 3D data segmentation

In the registration process, we superposed the CAD model with the 3D data of the part. But because we are interested in inspecting some specific surfaces, we need to segment the part into its different surfaces. The segmentation of the 3D cloud is done

by computing the distance between every 3D point and all of the surfaces in the CAD model (IGES format), and by comparing some local geometric properties between each 3D point in the cloud and its closest point on the surface. In the IGES CAD model, all the surfaces of the part are defined as a parametric NURBS (Non-Uniform Rational B-Splines) surfaces.

The problem of computing the distance from a 3D point to a NURBS surface can be formulated as finding a point on the parametric surface such that the distance between the 3D point and the point on the surface is minimal in the perpendicular direction to the tangent plane at the point on the surface. The problem is solved as a minimisation problem.

The local geometric properties that we estimate are: the normal surface, the gaussian curvature and the mean curvature. For the point on the parametric surface, those properties are estimated using the surface parameters (NURBS). For the 3D point, we use a parametric second order polynomial computed across a neighbourhood of points. A 3D point is labelled with the name (number) of the closest NURBS surface if the local geometric properties of the 3D point are similar to those on the parametric surface. A fonctional block diagram of the segmentation appears in Figure 2.

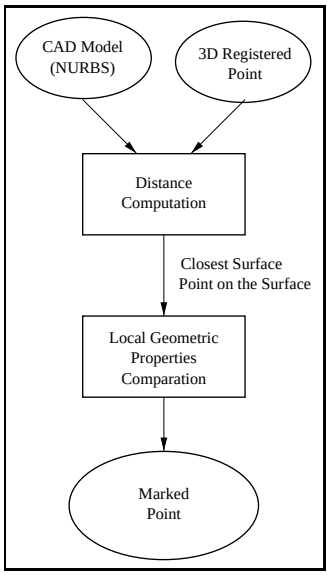

FIG. 2: *Block diagram of the point segmentation system*

5.1. *Point/NURBS surface distance computation*

The distance of a point to a NURBS surface can be computed as follow: find a point on the parametric space of the surface (u_0, v_0) such that the distance between the surface $\overrightarrow{s}(u_0, v_0)$ and the point $\overrightarrow{r}$ is minimum in a direction perpendicular to the

tangent plane at the point (see Figure 3).

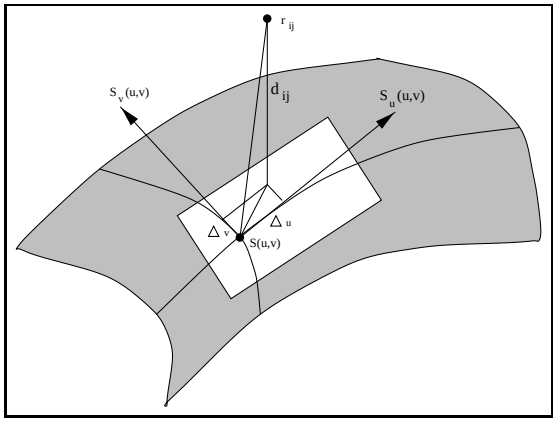

FIG. 3: *Point/NURBS surface distance*

The function to be minimized is the following:

$$min_{u_0,v_0} \|\overrightarrow{r} - \overrightarrow{s}(u,v)\|^2.$$

If one performs the Taylor expansion of the parametric surface $\overrightarrow{s}(u,v)$, we obtain:

$$\overrightarrow{s}(u,v) = \overrightarrow{s}(u_0,v_0) + \frac{\partial \overrightarrow{s}}{\partial u}(u_0 - u) + \frac{\partial \overrightarrow{s}}{\partial v}(v_0 - v)$$

where the derivatives are equal to:

$$\frac{\partial}{\partial u}\overrightarrow{s}(u,v) = \frac{AB-CD}{E^2} \text{ and } \frac{\partial}{\partial v}\overrightarrow{s}(u,v) = \frac{FB-GD}{E^2}$$

Where:

$$A = \sum_{i=0}^{n_i}\sum_{j=0}^{n_j} w_{ij}\overrightarrow{d_{ij}}\frac{\partial}{\partial u}N_i^k(u)N_j^l(v),$$

$$B = \sum_{i=0}^{n_i}\sum_{j=0}^{n_j} w_{ij}N_i^k(u)N_j^l(v),$$

$$C = \sum_{i=0}^{n_i}\sum_{j=0}^{n_j} w_{ij}\frac{\partial}{\partial u}N_i^k(u)N_j^l(v),$$

$$D = \sum_{i=0}^{n_i}\sum_{j=0}^{n_j} w_{ij}\overrightarrow{d_{ij}}N_i^k(u)N_j^l(v),$$

$$E = \sum_{i=0}^{n_i}\sum_{j=0}^{n_j} w_{ij}N_i^k(u)N_j^l(v),$$

$$F = \sum_{i=0}^{n_i}\sum_{j=0}^{n_j} w_{ij}\overrightarrow{d_{ij}}N_i^k(u)\frac{\partial}{\partial v}N_j^l(v),$$

$$G = \sum_{i=0}^{n_i}\sum_{j=0}^{n_j} w_{ij}N_i^k(u)\frac{\partial}{\partial v}N_j^l(v),$$

$$\frac{\partial}{\partial u}N_i^k(u) = \frac{k}{u_{i+k-1}-u_{i-1}}N_i^{k-1}(u) - \frac{k}{u_{i+k}-u_i}N_{i+1}^{k-1}(u) \text{ and}$$

$$\frac{\partial}{\partial v}N_j^l(v) = \frac{l}{u_{j+l-1}-u_{j-1}}N_j^{l-1}(v) - \frac{l}{u_{l+l}-u_j}N_{j+1}^{l-1}(v).$$

Using this expansion, the minimization problem becomes:

$$min_{u_0,v_0} \| \overrightarrow{r} - \overrightarrow{s}(u_0,v_0) - \frac{\partial \overrightarrow{s}}{\partial u}(u_0-u) - \frac{\partial \overrightarrow{s}}{\partial v}(v_0-v) \|^2.$$

This can be expressed in matrix from as:

$$min_{u_0,v_0} \| J\overrightarrow{w} - \overrightarrow{d} \|^2$$

where J is the Jacobien matrix of $\overrightarrow{s}(u,v)$ and is given by:

$$J = \begin{bmatrix} \frac{\partial s_x}{\partial u} & \frac{\partial s_x}{\partial v} \\ \frac{\partial s_y}{\partial u} & \frac{\partial s_y}{\partial v} \\ \frac{\partial s_z}{\partial u} & \frac{\partial s_z}{\partial v} \end{bmatrix}$$

and $\overrightarrow{w} = \begin{vmatrix} u_0 - u \\ v_0 - v \end{vmatrix}$ is equal to the variation of the parametrization.

If $\overrightarrow{d}(u,v)$ is the error for the initial parametrization (u_t, v_t), i.e. the initial closest point to the CAD format. Let: $\overrightarrow{d}(u,v) = \overrightarrow{r} - \overrightarrow{s}(u,v)$, then the solution to the minimization problem is equal to: $\overrightarrow{w}(J^T J)^{-1} J^T \overrightarrow{d}$. Using an iterative procedure, one can compute the distance of the point from the surface in less than four to five iterations.

5.2. *Geometric properties comparison*

Let P be a point from the 3D range data, and Q the closest point to P on the surface. To terminate the segmentation process, we estimate and compare some local geometric properties of P and Q. Geometric properties of Q are estimated using the NURBS CAD model.

We estimate the local geometric properties of P by using the method proposed by Boulanger [BOU 94]. This method is viewpoint invariant because the surface estimation process minimizes the distance between the surface NURBS surface $\overrightarrow{s}$ and the 3D data point in a direction perpendicular to the tangent plane of the surface at this point. The surface normal $\overrightarrow{n}(u,v)$, the gaussian curvature $K(u,v)$ and the mean curvature $H(u,v)$ for the point $P(u,v)$ from the parametric surface $\overrightarrow{\eta}(u,v)$ can be estimated by:

$$\overrightarrow{n}(u,v) = \frac{\overrightarrow{r_u}(u,v) \times \overrightarrow{r_v}(u,v)}{\| \overrightarrow{r_u}(u,v) \times \overrightarrow{r_v}(u,v) \|}$$

$$K(u,v) = \frac{[\overrightarrow{r_{uu}}\,\overrightarrow{r_u}\,\overrightarrow{r_v}][\overrightarrow{r_{vv}}\,\overrightarrow{r_u}\,\overrightarrow{r_v}] - [\overrightarrow{r_{uv}}\,\overrightarrow{r_u}\,\overrightarrow{r_v}]^2}{|\overrightarrow{r_u} \times \overrightarrow{r_v}|^4}$$

$$H(u,v) = \frac{A+B-2C}{2D^3}$$

where:

$$A = (\overrightarrow{r_u} \cdot \overrightarrow{r_v})[\overrightarrow{r_{uu}}\,\overrightarrow{r_u}\,\overrightarrow{r_v}],$$

$$B = (\overrightarrow{r_u} \cdot \overrightarrow{r_v})[\overrightarrow{r_{vv}}\,\overrightarrow{r_u}\,\overrightarrow{r_v}],$$

$$C = (\overrightarrow{r_u} \cdot \overrightarrow{r_v})[\overrightarrow{r_{uv}}\,\overrightarrow{r_u}\,\overrightarrow{r_v}],$$

$$D = |\overrightarrow{r_u} \times \overrightarrow{r_v}|,$$

$$[\overrightarrow{a}\ \overrightarrow{b}\ \overrightarrow{c}] = \overrightarrow{a} \cdot (\overrightarrow{b} \times \overrightarrow{c}), \text{ and}$$

$$\overrightarrow{r_u} = \frac{\partial \overrightarrow{r}}{\partial u}, \overrightarrow{r_v} = \frac{\partial \overrightarrow{r}}{\partial v}, \overrightarrow{r_{uu}} = \frac{\partial^2 \overrightarrow{r}}{\partial u^2}, \overrightarrow{r_{vv}} = \frac{\partial^2 \overrightarrow{r}}{\partial v^2} \text{ and } \overrightarrow{r_{uv}} = \frac{\partial^2 \overrightarrow{r}}{\partial u \partial v}.$$

We need to estimate the first and second partial derivatives at the point P by using a parametric second order polynomial. It is obtained by using a $N \times N$ neighborhood, where $\overrightarrow{r}(u,v) = (x(u,v), y(u,v), z(u,v))^T$ is the measured point from the range sensor .

Let $\overrightarrow{\eta}(u,v) = \sum_{i=0}^{2} \sum_{j=0}^{2} \overrightarrow{a_{ij}} u^i v^j = (h_x(u,v), h_y(u,v), h_z(u,v))^T$, where $\overrightarrow{a_{ij}}$ is the coefficient of each component of $\overrightarrow{\eta}(u,v)$ and equals to zero if $i+j > 2$. Using this polynomial the partial derivatives at the point P are:

$$\overrightarrow{\eta_u} = \overrightarrow{a_{10}} + 2\overrightarrow{a_{20}} u_0 + \overrightarrow{a_{11}} v_0,\ \overrightarrow{\eta_v} = \overrightarrow{a_{01}} + \overrightarrow{a_{11}} u_0 + 2\overrightarrow{a_{02}} v_0,$$
$$\overrightarrow{\eta_{uu}} = 2\overrightarrow{a_{20}},\ \overrightarrow{\eta_{vv}} = 2\overrightarrow{a_{02}}, \text{ and } \overrightarrow{\eta_{uv}} = \overrightarrow{a_{11}}$$

where (u_0, v_0) are the parametric coordinates in the center of the neighborhood. These parameters are found by using the least-square method.

Finally, we compare the local geometric properties of Q, estimated from the NURBS surface, to P from the 3D range data. Let α_{tol} be the permissible angle between the surface normal $\overrightarrow{N_s}$ and 3D data normal $\overrightarrow{N_r}$ at point P. Then the condition $|Angle(\overrightarrow{N_s}, \overrightarrow{N_r})| \leq \alpha_{tol}$ has to be respected. Let K_{tol} and H_{tol} be the defined variation of the gaussian and the mean curvatures, then the conditions: $|K_s - K_r| \leq K_{tol}$ and $|H_s - H_r| \leq H_{tol}$ have to be respected.

6. Visual inspection results

A high speed range sensor is used to digitize the parts. The sensor is mounted on a coordinate measuring machine to allow precise mechanical registration between views. The result of this digitization is an unordered serie of measurements describing the scanned object as illustrated in Figure 4.

For a rapid visualisation of the various defects in the part, we implemented a graphical user interface as shown in Figure 5. This figure illustrates the different actions that can be executed for a specific surface or for the whole part. This is the main window of the system. After the segmentation process, the surface of interest is chosen by specifying its label.

Figure 6 shows the cloud of 3D points resulting from the registration process of the 3D data with the CAD model, and some of its segmented surfaces.

Choosing *Intervalle Tolerance* (see Figure 5), the window displays the range containing all the points on the surface. We can change the limits of the window, and the system displays the points in the new range of tolerance with a different color for those out of the new tolerance range. For example, in Figure 6 (d) the tolerance range

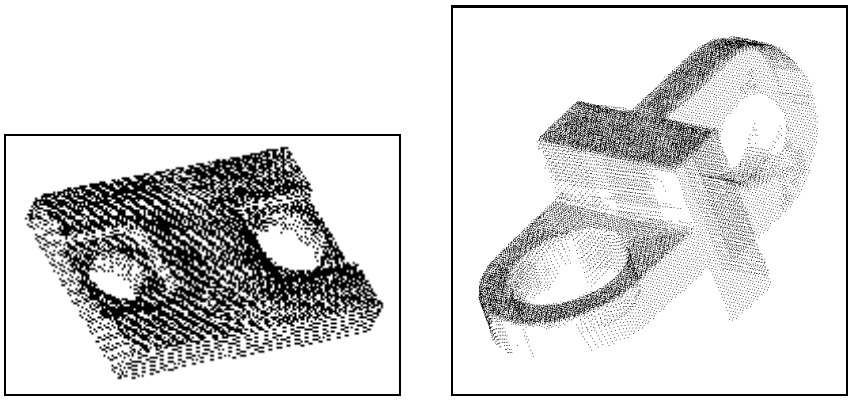

(a) 3D data of part one (b) 3D data of part two

FIG. 4: *3D data obtained from a NRCC range sensor*

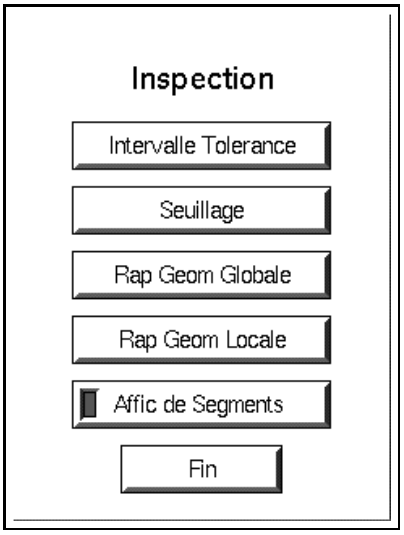

FIG. 5: *Graphical user interface for visual inspection - main window*

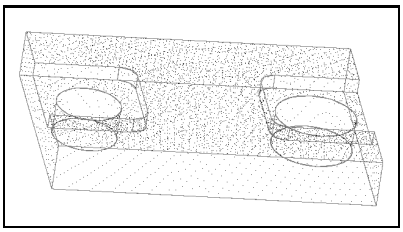

(a) Registration of part one

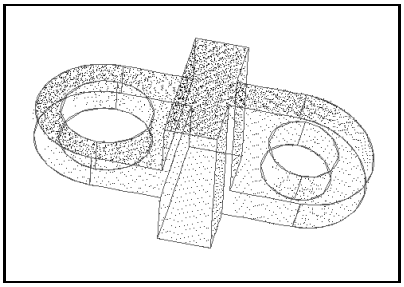

(b) Registration of part two

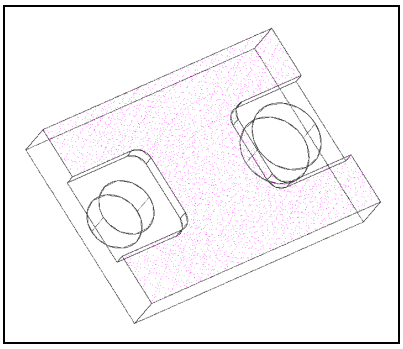

(c) Segmented surface of part one using *Intervalle Tolerance* $(-0.50mm, 0.71mm)$

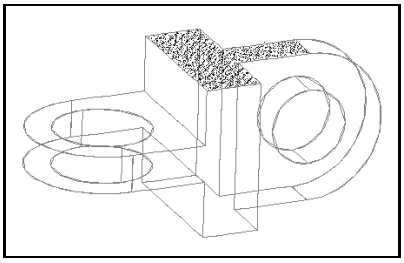

(d) Segmented surface of part two using *Intervalle Tolerance* $(-0.62mm, 0.41mm)$

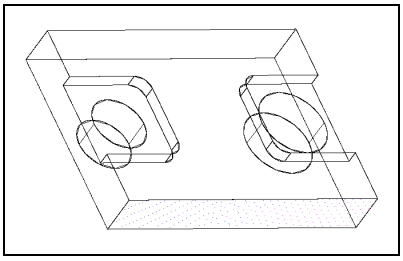

(e) Segmented surface of part one using *Seuillage* (threshold = 0.0mm)

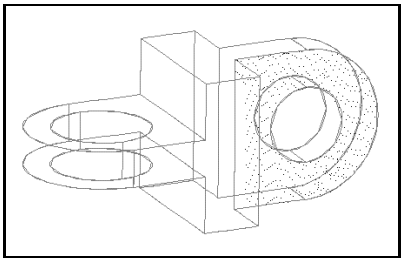

(f) Segmented surface of part two using *Seuillage* (threshold = 0.3mm)

FIG. 6: *Registration and segmented surfaces of two parts*

is $(-0.6214mm, 0.4128mm)$, and in Figure 8 (a), it is set to $(-0.2mm, 0.3mm)$. In Figure 8 (a) we have made an additional zoom in the system for a better visualization.

Selecting *Seuillage* (see Figure 5), we can specify a threshold value and the system displays the points under it, with a different color from those over the threshold. For example, in Figure 6 (e) the threshold was $0mm$. A high quality color picture show that the points under the threshold are on one side and the points over the threshold are on the other side, meaning that there is a small rotation, but since the tolerance range for this surface was low $(-0.1360mm, 0.0440mm)$, we argue that this rotation was artificially produced by the registration process.

The system allows two kinds of numerical reports, chosen from the main window (Figure 5): the option *Rap Geom Globale* and *Rap Geom Locale*. In Figure 7 we show the result from *Rap Geom Globale* for the surface 1 of the part two. This report is basically a statistical description of the surface (averages and dispersion values). The *Rap Geom Locale* outputs the values of the normal $\overrightarrow{n}$ of the gaussian curvature $K(u, v)$ and of the mean curvature $H(u, v)$, for each point in the segmented cloud of 3D points or for the nearest point on the surface.

```
 RAPPORT DE TOLERANCES  SURFACE 1


Nombre de Points:                        1811
Nombre de Points Aberrants:              240
Nombre de Points non-aberrants:          1571
Moyenne Arithmetique (p n-a):            -0.00112962
Variance (sigma^2):                      0.00141705
Ecart Type (sigma) :                     0.0376438
Valeur Minimum:                          -0.0965725
Valeur Maximum:                          0.0991523
```

FIG. 7: *Statistical description of the surface 1 of part two*

Finally, the last option in the main window is *Affic de Segments*. This option shows the visual results in both *Range Tolerances* and *Seuillage*. Results are displayed as a linear segment between the 3D point in the segmented cloud and the nearest point on the surface. Using this option we can better visualize some defects on the part, as shown in Figure 8 (b), where a problem of flatness is detected. In Figure 8 (a) a zoom of the color picture of the same surface is displayed. Similarly, in Figure 8 (d), a problem of circularity on the part two is detected.

7. Conclusion

We have introduced a visual inspection system for manufactured parts. The system first registers a cloud of 3D points with a triangulated STL CAD model of the part, and then segments the 3D points in their respective surface by employing the NURBS IGES CAD model. Results of inspection are available in two ways: visually, using a

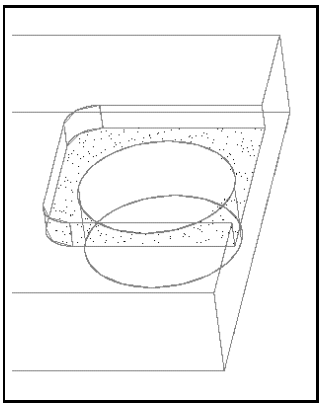

(a) Segmented surface of part one using a color map

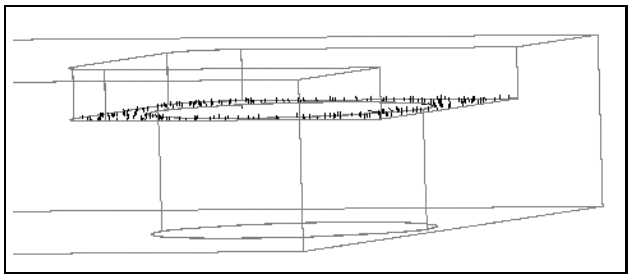

(b) Segmented surface of part one using *Affic de Segments*

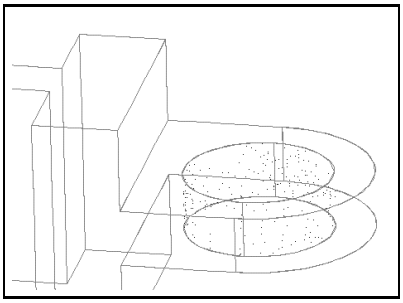

(c) Segmented surface of part two using a color map

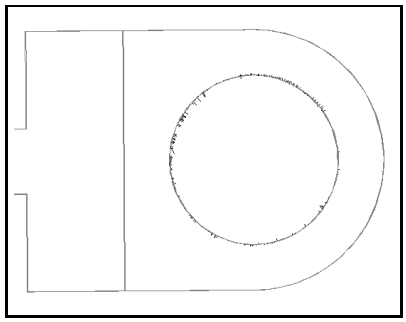

(d) Segmented surface of part two using *Affic de Segments*

FIG. 8: *Visual inspection results using color map and segment display options*

color map to display the level of discrepancy between the measured points and the CAD model, and a hardcopy report with a statistical description of the surface under inspection.

In spite of the apparently simple geometrical form of the parts that we use, they are useful because they all show some symmetries, making the registration process more difficult. More complex is the shape of the inspected part, more easy is it to find the transformation to register the 3D data with the CAD model.

The segmentation process is not dependent of the part geometry. It depends basically on the 3D points precision and in a most important way on the density of points on a segmented surface, in order to obtain a good estimate of the local geometrical properties.

The precision in the inspection results is mainly function of the accuracy of the 3D points. At present we find some range sensors with a high precision, but in order to approach the accuracy of a coordinate measuring machine, it is necessary to improve either the sensor hardware or the digitization process by defining the best sensor placements.

An important extension of this work is to implement an algorithm to analyze the geometrical tolerance by using the local geometrical properties obtained for each point in the segmentation process. In effect, in the inspection of geometric tolerances, often it is necessary to compare certain characteristics of a surface with respect to another surface. Therefore, we could use the segmentation result to make geometric tolerance control.

Bibliographie

[BER 95] BERALDIN J., EL-HAKIM S. and BLAIS F., "Performance evaluation of three active vision systems built at the NRC", *Proceedings of the Conference on Optical 3-D Measurement Techniques*, p. 352–362, Vienna, Austria, 2-4 October 1995.

[BES 92] BESL P. and MCKAY N., "A Method for Registration of 3D Shapes", *IEEE Transactions on Pattern Analysis and Machine Intelligence*, vol. 14, n° 2, p. 239–256, February 1982.

[BOU 94] BOULANGER P., "Extraction multiéchelle d'éléments géométriques", Ph.D. Dissertation: Génie Electrique, Université de Montreal, Canada, 226 p., 1994.

[BOU 96] BOULANGER P., MORON V. and REDARCE H., "High-speed and non-contact validation of rapid prototyping parts", *SPIE's Rapid Product Development Technologies*, p. 46–60, Boston, Mass. U.S.A, 18-19 November 1996.

[CHI 82] CHIN R. and HARLOW C., "Automated visual inspection : A survey", *IEEE Transactions on Pattern Analysis and Machine Intelligence*, vol. PAMI-4, n° 6, p. 557–573, 1982.

[MAR 91] MARSHALL A., MARTIN R. and HUTBER D., "Automatic inspection of mechanical parts using geometric models and laser range finder data", *Image and Vision Computing*, vol. 9, n° 6, p. 385–405, December 1991.

[MAS 95] MASUDA T. and YOKOYA N., "A Robust Method for Registration and Segmentation of Multiple Range Images", *Computer Vision and Image Understanding*, vol. 61, n° 3, p. 295–307, 1995.

[MOR 96] MORON V., BOULANGER P., MASUDA P. and REDARCE H., "High speed optical inspection of rapid prototyping parts", *European Symposium on Lasers, Optics, and Vision for Productivity in Manufacturing I*, Besançon, France, 10-14 June 1996.

[MOR 96b] MORON V., BOULANGER P., REDARCE H. and JUTARD A., "Mise en correspondance du modèle CAO d'un objet avec son image 3D: Application à l'inspection", *RFIA'96, Congrès de Reconnaissances de Formes et Intelligence Artificielle*, p. 913–922, Rennes, France, 16-18 Janvier 1996.

[NEW 95] NEWMAN T. and JAIN A., "A survey of automated visual inspection", *Computer Vision and Image Understanding*, vol. 61, n° 2, p. 231–262, March 1995.

[NEW 95b] NEWMAN T. and JAIN A., "A system for 3D CAD-based inspection using range images", *Pattern Recognition*, vol. 28, n° 10, p. 1555–1574, 1995.

[RIO 84] RIOUX M., "Laser range finder based on synchronized scanners", *Applied Optics*, vol. 23, n° 21, p. 3837–3844, November 1984.

[RIO 87] RIOUX M., BECHTHOLD G., TAYLOR D. and DUGGAN M., "Design of a large depth of view three-dimensional camera for robot vision", *Optical Engineering*, vol. 26, n° 12, p. 1245–1250, 1987.

[RIO 97] RIOUX M., "Laser range finder based on syncronized scanners", *SPIE Milestone Series, Optical Techniques for Industrial Inspection*, p. 142–149, Bellinghan, U.S.A., 1997.

[ROU 87] ROUSSEEUW P. and LEROY A., *Robust Regression & Outlier Detedtion*. John Wiley & Sons. New York, 1987.

[TAR 95] TARBOX G. and GOTTSCHLICH S., "IVIS: An integrated volumetric inspection system", *Computer Vision and Image Understanding*, vol. 61, n° 3, p. 430–444, May 1995.

[TRU 94] TRUCCO E., DIPRIMA M. and ROBERTO V., "Visibility scripts for active feature-based inspection", *Pattern Recognition Letters*, vol. 15, p. 1151–1164, 1994.

[TRU 97] TRUCCO E., UMASUTHAN M., WALLACE A. and ROBERTO V., "Model-based planning of optimal sensor placements for inspection", *IEEE Transactions on Robotics and Automation*, vol. 13, n° 2, p. 182–194, April 1997.

Annexe I

French title: Système visuel pour l'inspection rapide et automatisée de pièces 3D.

English title: Visual system for fast and automated inspection of 3D parts.

Short english title: Visual system for 3D inspection.